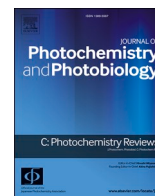


Contents lists available at [ScienceDirect](https://www.sciencedirect.com)

# Journal of Photochemistry & Photobiology, C: Photochemistry Reviews

journal homepage: [www.elsevier.com/locate/jphotochemrev](http://www.elsevier.com/locate/jphotochemrev)

## Optical trapping in micro- and nanoconfinement systems: Role of thermo-fluid dynamics and applications

Tetsuro Tsuji<sup>a,b,\*</sup>, Kentaro Doi<sup>c</sup>, Satoyuki Kawano<sup>d,\*</sup><sup>a</sup> Department of Advanced Mathematical Sciences, Graduate School of Informatics, Kyoto University, Yoshida-honmachi, Sakyo-ku, Kyoto 606-8501, Kyoto, Japan<sup>b</sup> Research Project of Fluid Science and Engineering, Advanced Engineering Research Center, Kyoto University, Yoshida-honmachi, Sakyo-ku, Kyoto 606-8501, Kyoto, Japan<sup>c</sup> Department of Mechanical Engineering, Toyohashi University of Technology, 1-1 Tempaku-cho, Toyohashi 441-8580, Aichi, Japan<sup>d</sup> Department of Mechanical Science and Bioengineering, Graduate School of Engineering Science, Osaka University, 1-3 Machikaneyama-cho, Toyonaka 560-8531, Osaka, Japan

### ARTICLE INFO

#### Keywords:

Microfluidics  
Nanofluidics  
Optofluidics  
Fluid mechanics  
Photothermal effects  
Microelectromechanical systems

### ABSTRACT

In this mini-review, recent advances on the role of a focused laser in micro- and nanofluidic systems is widely introduced with special interest in thermo-fluid dynamical aspects and their importance in optical manipulation. As a brief introduction to microfluidic systems, we describe the advantages and challenges of the use of micro- and nanoscale confinement in optical trapping, as well as standard fabrication techniques for micro- and nanofluidic systems. From thermo-fluid dynamical viewpoints, various phenomena that accompany a laser irradiation to fluidic devices, are explained in detail. These phenomena can affect the optical trapping of target materials significantly, and are classified into two categories: one that induces the fluid flow around the target and another that directly acts on it as an external force. These classes are reviewed by shedding light on some recent cutting-edge researches for optical manipulation. Some applications using thermo-fluid dynamics in microfluidic systems for the measurement of optical forces and for the separation, measurement, and detection of target materials are also introduced.

### 1. Introduction

Controlling the motion of micro- and nanoscale materials has been one of the key techniques in bioscience and nanoengineering. For instance, nanofluidic devices can identify deoxyribonucleic acid (DNA) bases by measuring the modulation of electrical signals that are triggered by the motion of the DNA molecules in nanoscale channels with embedded sensing electrodes [1]. In such applications, target materials have to be transported to a sensing part with desired speed and frequency. However, due to the smallness of targets and devices, achieving these requirements with high precision is not a simple task and needs some specialized tools.

Optical tweezers (or optical trapping), notably pioneered by Ashkin and his coworkers [2–7], are a manipulation technique using a focused laser beam illuminated on a target material. Ashkin reported the acceleration and trapping of microparticles by optical radiation pressure [2]. He and his collaborators [3,5] successively demonstrated optical

manipulations of yeast cells and microparticles in a living cell of a spirogyra. It was marvelous that biological cells, as well as micro- and nanoparticles, could be optically manipulated without touching.

Because of its non-contact and non-invasive nature, the optical tweezers have contributed significantly to various research fields that require precise control on the motion of micro- and nanoscale materials. With the help of available references such as textbooks and review articles (see, e.g., [8,9]) and commercial experimental apparatus, the optical trapping experiments have been carried out not only by the researchers in optics fields but also by those who do not specialize in optics. Microfluidics and nanofluidics, where a fluid containing molecules and/or colloids is confined in micro- and nanoscale fluidic channels, are the research fields that enjoy the benefits of optical tweezers. This mini-review aims to introduce some recent advances of optical-force-mediated and/or optical-effect-mediated novel manipulation techniques of micro- and nanoscale targets in fluidic devices and/or confinements.

\* Corresponding authors.

E-mail addresses: [tsuji.tetsuro.7x@kyoto-u.ac.jp](mailto:tsuji.tetsuro.7x@kyoto-u.ac.jp) (T. Tsuji), [kawano@me.es.osaka-u.ac.jp](mailto:kawano@me.es.osaka-u.ac.jp) (S. Kawano).<sup>1</sup> ORCID: 0000-0002-2087-5459<https://doi.org/10.1016/j.jphotochemrev.2022.100533>

Received 29 October 2021; Received in revised form 27 April 2022; Accepted 30 April 2022

Available online 10 May 2022

1389-5567/© 2022 The Author(s). Published by Elsevier B.V. This is an open access article under the CC BY license (<http://creativecommons.org/licenses/by/4.0/>).

First, quick overviews of optical forces and microfluidic systems will be given in Secs. 2 and 3, respectively, for those without the background of optical trapping and/or microelectromechanical systems (MEMS) technologies. In Sec. 4, some important effects in thermo-fluid dynamics caused by laser irradiation are described, with a particular focus on recent advanced researches. This knowledge is useful in the appropriate understandings of optical-trapping experimental data, which inherently include the effects of surrounding fluid flows and temperature fields. In Sec. 5, we introduce some recent applications related to optical trapping and the effects of focused lasers on microfluidic systems.

## 2. Quick overview of optical forces

For a microparticle that is much larger than the wavelength of light, optical pressure is understood within the framework of ray optics or geometrical optics, as constructed by Ashkin [10]. As shown in Fig. 1, a ray partially reflects and refracts at a surface when a ray of power  $P$  hits a spherical surface. Let us consider the ray of an incident angle  $\theta$  with the incident momentum per second  $n_1P/c$ , where  $n_1$  and  $c$  are the index of refraction of fluid and the speed of light, respectively. The optical force exerted on the sphere is expressed by the sum of power  $PR$  and the multiply refracted rays with powers of  $PT^2$ ,  $PT^2R$ , and  $PT^2R^n$ , where  $R$  and  $T$  denote refraction and transmission coefficients, respectively [11]. As a result, optical forces along the optical axis and perpendicular to the axis are optical scattering force  $F_{\text{scat}}$  and gradient force  $F_{\text{grad}}$ , respectively, as follows:

$$F_{\text{scat}} = \frac{n_1P}{c} \left\{ 1 + R\cos 2\theta - \frac{T^2[\cos(2\theta - 2r) + R\cos 2\theta]}{1 + R^2 + 2R\cos 2r} \right\}, \quad (1)$$

and

$$F_{\text{grad}} = \frac{n_1P}{c} \left\{ R\sin 2\theta - \frac{T^2[\sin(2\theta - 2r) + R\sin 2\theta]}{1 + R^2 + 2R\cos 2r} \right\}. \quad (2)$$

The net force is obtained by superposing all individual rays. For instance, a polystyrene particle in water has a relative index of refraction of about 1.2, and thus a microparticle exposed to a focused light is attracted to the focal point along with both the axial and radial directions.

On the other hand, metallic nanoparticles are often much smaller than the wavelength of light and have large polarizability  $\alpha$  (see, e.g., [12,13]). The optical trapping of metallic nanoparticles is understood based on the Rayleigh scattering theory. Assuming a point-like dipole particle, the induced polarization is expressed by  $\mathbf{P} = \alpha\mathbf{E}$ , where  $\mathbf{E}$  denotes the induced electric field. In the Rayleigh regime, the net optical

force acting on the nanoparticle is divided into two components [4,14,15] such as

$$\mathbf{F} = \mathbf{F}_{\text{grad}} + \mathbf{F}_{\text{scat}}. \quad (3)$$

The gradient force  $\mathbf{F}_{\text{grad}}$  is expressed by

$$\mathbf{F}_{\text{grad}} = \frac{\alpha}{2} \nabla \langle \mathbf{E}^2 \rangle, \quad (4)$$

where the bracket corresponds to the time average over an optical cycle [14]. Assuming a point dipole, the polarizability  $\alpha$  is represented by

$$\alpha = 4\pi\epsilon_0 n_1^2 a^3 \left( \frac{m^2 - 1}{m^2 + 2} \right), \quad (5)$$

where  $\epsilon_0$  is the permittivity of vacuum,  $a$  is the radius of particle, and  $m = n_2/n_1$  is the fraction of the index of refraction of particle  $n_2$  to that of the surrounding medium  $n_1$  [16]. The scattering force is [14]

$$\mathbf{F}_{\text{scat}} = \frac{8\pi n_1 k^4 a^6}{3c} \left( \frac{m^2 - 1}{m^2 + 2} \right)^2 \langle \mathbf{S} \rangle, \quad (6)$$

where  $\mathbf{S}$  is the Poynting vector and  $k = 2\pi n_1/\lambda$  is the wave number of the light of the wavelength  $\lambda$ . In the Rayleigh regime, it is found that the forces  $\mathbf{F}_{\text{grad}}$  and  $\mathbf{F}_{\text{scat}}$  are proportional to  $a^3$  and  $a^6$ , respectively, and that  $\mathbf{F}_{\text{grad}}$  against the direction of incident light is required to be greater than  $\mathbf{F}_{\text{scat}}$  for stable trapping. The objective lens with a high numerical aperture (NA) is effective to increase the gradient strength [14]. As the particle size increases, the optical force is no longer described by the Rayleigh scattering and then the Lorenz-Mie scattering theory is suitable to express the phenomena [4,10,17–19].

## 3. Quick overview of microfluidic systems

Microfluidic systems have the length scale of micrometers which is, practically, between several micrometers and hundreds of micrometers. When the length scale is downsized to sub-micrometers, the system is often called nanofluidics [20]. As will be described later in Sec. 3.2, fabrication techniques are different between micro- and nanofluidics because of physical limitations; usually the former is cheaper and rather well-established, but the latter costs high and needs many struggles. In this mini-review, we introduce a standard setup that is useful in optical trapping experiments, leaving more details and applications to a textbook [21].

### 3.1. Advantages and challenges

In optical trapping, confining a sample solution with dispersed small objects in micro- or nanofluidic systems has some advantages compared with experiments in bulk. First of all, a confinement can greatly reduce undesired and unexpected fluid motion, whatever its cause may be. The undesired flows easily occur during experiments due to, e.g., environmental disturbance, the deformation of channels, or thermal convection (see also Sec. 4). Evaluating and reducing the effect of background fluid flow is important in the precise measurement of optical forces acting on targets.

The confinement also plays a role in reducing a physical dimension. For instance, when a laser is irradiated to a microscale slit in such a way that the beam axis is perpendicular to the slit walls, the motion of the target with the size comparable to that of the slit can be regarded as quasi-planar. That is, the particle is allowed to move only in the plane parallel to the slit walls. In this case, the escape of the target from the trapping potential is suppressed in the beam propagation direction. Such quasi-two-dimensional trapping is useful when an objective lens with a high NA is not available, e.g., because of a thick substrate.

Another minor merit comes from the fact that the well-controlled background flow facilitates experiments. We can stop the flow during

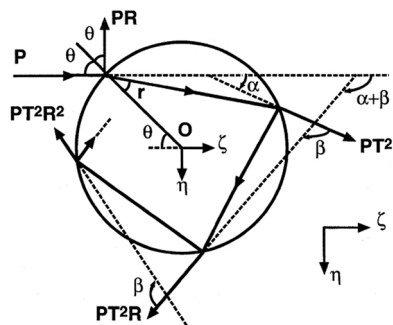


**Fig. 1.** Schematic diagram and coordinate system to determine the scattering and gradient forces that result from the multiple reflections and refractions of a single ray incident on a microsphere.  $\theta$  and  $r$  are the incident and refraction angles, respectively.  $R$  and  $T$  are the polarization-dependent Fresnel reflection and transmission coefficients, respectively.  $\eta$  and  $\zeta$  result in the direction of the gradient and scattering forces, respectively.

Reprinted with permission from [11]. Copyright 1996, The Laser Society of Japan.

data acquisition, e.g., video recording of optical trapping. After the acquisition, inducing a one-way background flow can replace the old solution with a new, fresh, and homogeneous one. In this way, the number of trials can be increased efficiently. Moreover, one does not have to wait for a target to diffuse to the laser focus but can force it to come to the focus.

Furthermore, microfluidics is well compatible with other optical tools. For instance, flow measurements in micro- and nanofluidics are fundamental techniques, and thus improving their resolutions and reducing costs are important for applications. If camera imaging is unnecessary for the measurement, an installation cost can be greatly reduced. A flow measurement technique based on fluorescence and photodetectors without camera imaging is developed in [22,23]. In this way, the microfluidic system is suitable for more integrated experimental systems.

Although the micro- and nanofluidic devices have the advantages as above, there are quite a lot of challenges to be overcome. For instance, nanofabrication technologies have been mainly developed for silicon substrates, which are not transparent and not suitable for laser irradiation. Transparent glass substrates are also available (e.g., [24]), but the thickness is, usually, not a standard 0.17 mm of coverslips. That is, a high-NA oil immersion lens is not applicable because of its short working distance. Below, we briefly introduce standard fabrication techniques and their difficulties.

### 3.2. Fabrication

Microfluidics needs the fabrication of microchannels, which may look difficult for those who never tried. In fact, there are many difficulties if one tries to make them from scratch, but there are "recipes" to follow (e.g., [21]). Here, a very standard one is introduced shortly. The dimensions of the narrowest part are usually larger than  $\sim 5 \mu\text{m}$  in microfluidic channels. In this case, the combination of SU-8 mold and polydimethylsiloxane (PDMS) demolding is popular.

First, the SU-8 mold is fabricated by a photolithography technique as follows. The SU-8 liquid is a negative photoresist and is cured upon light exposure. This photoresist is spincoated on a silicon substrate (Fig. 2(a)), and then the light exposure is made through a photomask that has the pattern of the fluidic channel (Fig. 2(b)). Therefore, after washing out the uncured photoresist (i.e., development), the convex pattern of cured SU-8 remains on the substrate (Fig. 2(c)). Note that the height of the mold is determined by the thickness of the coated SU-8 liquid film. The resolution of the width of the mold is mainly restricted by two factors: the wavelength of the exposure light, and the distance between the coated SU-8 film and the photomask. A standard light-exposure apparatus gives the minimum resolution around  $\sim 5 \mu\text{m}$ .

Second, a PDMS liquid is poured into the SU-8 mold (Fig. 2(d)). Then, the PDMS is cured upon heating. The cured PDMS is peeled off and de-molded from the SU-8 mold (Fig. 2(e)). The resulting cured PDMS has the concave pattern of the fluidic channel. Finally, the patterned face of the PDMS is attached to a glass substrate (Fig. 2(f)), after fabricating inlet and outlet holes. There is no need for a bonding agent because of the self-adsorption property of the PDMS. For more robust bonding between the PDMS and the substrate, a surface treatment by oxygen plasma exposure or ultraviolet light exposure is recommended.

The above process is rather easy and costs low. However, due to the low rigidity of the cured PDMS, the low-aspect-ratio (height/width) channel tends to collapse easily. Therefore, the channel height, which is determined by the thickness of the SU-8 liquid film, should be at least a couple of micrometers.

For smaller scale fabrication, the photolithography is not available due to the limitation of exposure light's wavelength and the proximity of the photomask and the substrate. Electron beam lithography is thus used to fabricate finer patterns of the fluidic channel. Roughly speaking, the process in Fig. 2(b) is replaced by electron beam exposure of a positive resist coated on a quartz glass. After development, a nanochannel is

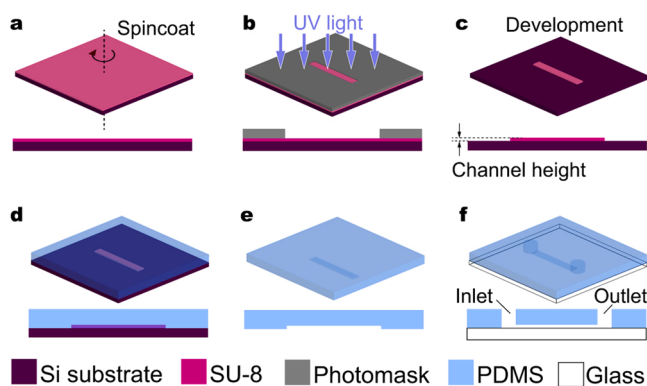


**Fig. 2.** Schematic of microchannel fabrication. (a) SU-8 liquid film is spincoated. (b) UV light exposure is made through a photomask. (c) Development is done to wash out uncured SU-8. (d) PDMS liquid is poured and cured. (e) Cured PDMS is peeled off from the SU-8 mold. (f) De-molded PDMS block is attached to a glass substrate, after fabricating holes for inlet and outlet.

formed by reactive ion etching. Nanoscale fluidic channels have huge hydraulic resistance. Therefore, injection of a sample solution by external pressure can collapse the channel. To avoid this collapsing, larger-scale microchannel connections between nanochannels and inlets are helpful (see, e.g., Fig. 3). Fig. 3 is an example of nanofluidic device. Only the part indicated as "nanochannel area" has nanoscale dimensions: other parts have microscale dimensions to reduce hydraulic resistance. Quartz glass bonding [20] is also useful to make nanofluidic devices robust to external pressure. However, the cost and time of fabricating these nanoscale fluidic devices are larger than those of microscale devices, and this difficulty often discourages laboratory-scale trials and errors. Therefore, a large amount of effort, training, and experiences are necessary for systematic experiments in nanofluidic devices.

### 4. Optical effects in thermo-fluid dynamics

Recent advances in plasmonic tweezers toward dynamic manipulation [26] and thermoplasmonics for fluid actuation [27] clearly elevate the importance of thermo-fluid dynamics. The optical effects in thermo-fluid dynamics can be roughly divided into two types: those acting on fluids (e.g., water solvent) and those acting on dispersed

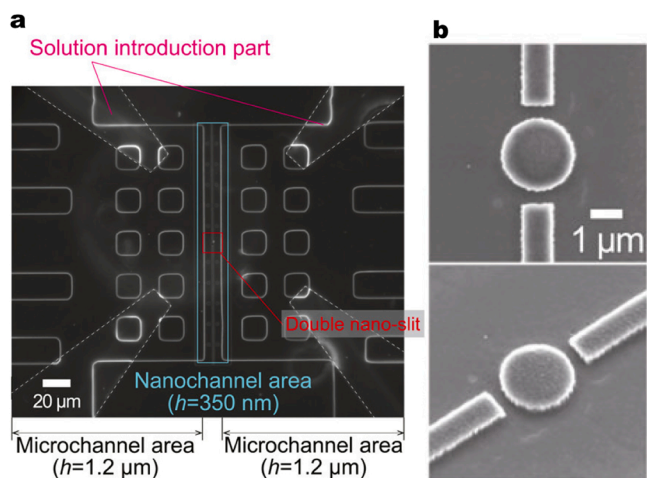


**Fig. 3.** Example images of nanofluidic devices. (a) Dark-field microscopy and (b) scanning electron microscopy images of a double-slit nanofluidic device used in [25]. Microchannels are used as solution introduction parts and are connected by nanochannels indicated as double nano-slit. Copyright 2021, American Chemical Society. Reprinted with permission from [25].

objects (e.g., nanoparticles). The former drives the fluid flow, yielding the flow drag acting on the dispersed objects; the latter directly acts on the object as external forces. When the magnitude of these forces is comparable to that of the optical forces, special care is required for optical trapping. As an introductory textbook for thermo-fluid dynamics in microfluidics, readers are referred to [28].

#### 4.1. Laser-induced fluid motion

##### 4.1.1. Theoretical background for thermo-fluid dynamics

Photothermal effects can generate a temperature field in a fluid. Usually, since the density of a fluid is temperature-dependent, the gravity exerts a buoyancy force acting on the fluid, yielding thermal convection. Fig. 4 describes the schematic of thermal convection in optical trapping. The basic equation of thermo-fluid dynamics that describes such a situation is the Navier-Stokes equation with the Boussinesq approximation (see, e.g., [29]). In a time-independent case, it is written as

$$\nabla \cdot \mathbf{u} = 0, \quad (7a)$$

$$\rho(\mathbf{u} \cdot \nabla) \mathbf{u} = -\nabla p + \mu \nabla^2 \mathbf{u} - \beta_0(T - T_0)\rho \mathbf{g}, \quad (7b)$$

$$\rho C_p(\mathbf{u} \cdot \nabla) T = \kappa \nabla^2 T + q, \quad (7c)$$

where  $\mathbf{u}$  is the flow velocity vector,  $\rho$  is the fluid density at a reference temperature  $T_0$ ,  $p$  is the pressure,  $\mu$  is the fluid viscosity,  $\beta_0$  is the thermal-expansion coefficient at temperature  $T_0$ ,  $T$  is the temperature of the fluid,  $\mathbf{g}$  is the acceleration of gravity,  $C_p$  is the specific heat at constant pressure,  $\kappa$  is the thermal conductivity of the fluid, and  $q$  is the heat generated by the photothermal effect. The third term in the right hand side of Eq. (7b) is the buoyancy force. Note that a small temperature variation, i.e.,  $\Delta T = |T - T_0| \ll T_0$ , is assumed. Moreover, for simplicity, the effect of the presence of particles on the fluid motion is not considered. Equation (7) contains the unknown functions  $\mathbf{u}$ ,  $p$ , and  $T$ , and can be solved numerically and self-consistently. For the theoretical formulation of thermal convection, e.g., the mathematical basis of Boussinesq approximation or physical meaning of Rayleigh numbers, the readers may be referred to a standard textbook in fluid mechanics [29] or a more specialized one for thermal convection [30].

Once the flow field  $\mathbf{u}$  is obtained, the drag force acting on the particles can be computed as  $6\pi a\mu\mathbf{v}$ , where  $a$  is the radius of particle and  $\mathbf{v}$  is a relative velocity of the fluid to the particle. For instance, if a typical numerical values in microscale experiments  $\eta \approx 10^{-3}$  Pa s,  $a \approx 0.5$   $\mu\text{m}$ ,  $|\mathbf{v}| \approx 10$   $\mu\text{m s}^{-1}$  are used, the drag force is estimated as  $\approx 100$  fN, which

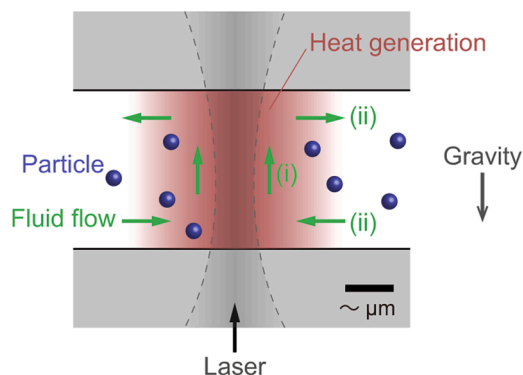


**Fig. 4.** Sketch of thermal convection in optical trapping. The laser is absorbed to a solvent and heat is generated. (i) Low density fluid goes up because of a buoyancy force. (ii) Horizontal flows must occur due to the mass conservation. In addition to optical forces, suspended particles are subject to a drag force and a thermophoretic force (see, Sec. 4.2.2) in such a situation. The drag force is described as  $6\pi a\mu\mathbf{v}$ , where  $a$  is a radius of the particle,  $\mu$  is a viscosity, and  $\mathbf{v}$  is a relative velocity of the fluid to the particle.

may be comparable to the optical forces. However, if the (relative) flow velocity could be reduced to  $|\mathbf{v}| \approx 0.1$   $\mu\text{m s}^{-1}$ , the drag force becomes now  $\approx 1$  fN, which may be negligible compared with the optical force. To suppress the flow velocity, the use of microfluidic device works successfully. For instance, it was estimated that the local temperature increase of  $\approx 50$  K in water solution resulted in the thermal convection with magnitude  $< 0.1$   $\mu\text{m s}^{-1}$  in a microchannel with a height of 17  $\mu\text{m}$  [31]. Note that the coupling between the fluid and particle motion is necessary for more accurate description of the phenomena. However, this coupling requires the treatment of moving boundaries, i.e., the sphere surfaces, in solving Eq. (7), and is usually much more difficult compared with Eq. (7) only.

Finally, let us remark the temperature increase of water induced by laser irradiation. In optical trapping, the wavelength of 1064 nm is frequently used for a trapping laser. The absorption coefficient of water [32] at this wavelength is not significant; for instance, a focused laser using a high NA objective (NA = 1.35, 100 $\times$  magnification) results in the temperature rise of  $\approx 1$  K [33] when a laser power after the objective is 50 mW. For this reason, this wavelength is preferred when thermal damage should be avoided, such as in biological experiments. On the other hand, water tends to absorb the wavelength close to 1.5  $\mu\text{m}$  (see, e.g., [34,35]).

##### 4.1.2. Thermally-induced fluid flows

The laser-induced thermal convection in a microscale slit is investigated in [34], where the temperature field is produced because of the photothermal effect of a water solvent. The flow velocity field analysis using particle image velocimetry (PIV) and a numerical simulation based on Eq. (7) are used to characterize the fluid flows, where the results are schematically shown in Fig. 5. Here, the heat generation  $q$  in Eq. (7c) is modeled as  $q = A_c I$ , where  $A_c$  is the absorption coefficient of water and  $I$  is the laser intensity distribution. The magnitude of the laser-induced thermal convection is strongly dependent on the length scale of the confinement (e.g., channel height [35]). Therefore, the resulting drag force acting on dispersed particles is also affected by the length scale of confinement, as exemplified in Sec. 4.1.1. When the confinement is weak, thermophoretic forces (see Sec. 4.2.2 below) and the fluid drag due to thermal convection often become comparable [35, 36]. The laser-induced thermal convection is usually axis-symmetric. However, applying a magnetic field to the dispersion of magnetic nanoparticles, the non-axis-symmetric states may occur in the laser-induced thermal convection [37].

Instead of the photothermal effect of the solvent as described above, plasmonic heating [38] can be utilized to localize the high-temperature region. In [27], the monolayer of gold nanorods is illuminated by the laser, and the resulting heat generates thermal convection. This convection can be used as fluid actuation in a microfluidic circuit. Such plasmonic-heating-mediated methods for the generation of temperature field have been reported in various articles; some of them will be also introduced in subsequent parts of this paper.

Thermal convection can be actively used to collect target particles near a heated region. In [39], bacteria are accumulated at the stagnant area of the convective flow. By the use of partially-Au-coated particles as a heat source, the thermal damage to the assembled bacteria is avoided. In [40,41], additional external electric fields are applied to induce electrothermal flows [40] and electroosmotic flows [41] to realize nanoparticle tweezers.

It should be remarked that an inhomogeneous temperature field can induce fluid flows, thermoosmotic flows [42,43], even under the absence of gravity. (Recall that gravity is necessary for thermal convection.) Thermoosmotic flows are observed experimentally near a solid-liquid interface heated by a photothermal effect of Au nanoparticle [44] and are also investigated numerically for both light-absorbing particles and solvents [45]. This flow is considered as the origin of self-thermophoresis of Janus particles [46–48] or spheroidal nanoparticles [49], which have temperature distribution around their

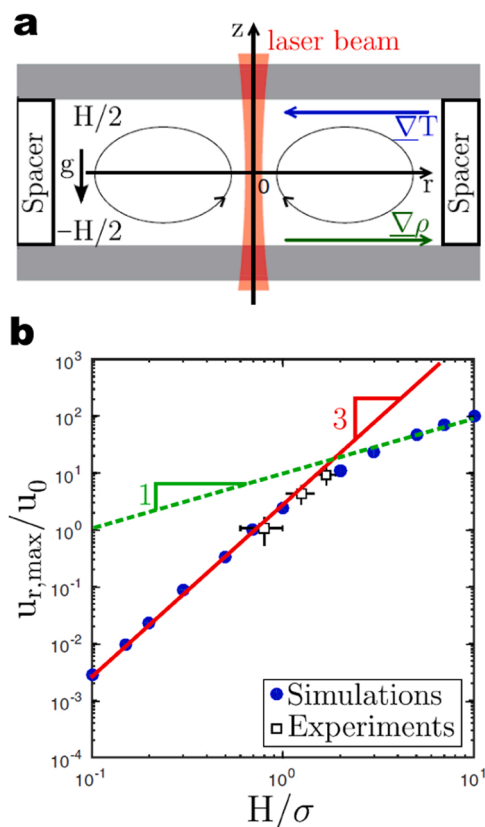


**Fig. 5.** (a) The schematic of the experiment in [34] and (b) the magnitude of laser-induced thermal convection  $u_{r,\max}$  as a function of a channel height  $H$ . Normalization factors in the vertical and horizontal axes, i.e.,  $u_0$  and  $\sigma$ , are a reference speed that balances the viscous term and the buoyancy force and a characteristic width of temperature field, respectively. Copyright 2016, American Physical Society.

Reprinted with permission from [34].

surfaces upon laser illumination. The thermoosmotic flow around a Janus particle is investigated in [46]. A Janus particle is heated by laser irradiation, as shown in Fig. 6(a), and the resulting flow is experimentally evaluated (Fig. 6(b)) and also is simulated (Fig. 6(c)).

As a fluid actuation method, Marangoni flows, the class of flows induced at an interface of two different fluids due to surface tension gradient (see, e.g., [28]), have practical feasibility. Photothermal effects can induce Marangoni flows because surface tension is usually dependent on temperature. A bubble may be created upon plasmonic heating of gold nanostructures. Along the surface of the created bubble, the Marangoni flow occurs and the fluid transport can be achieved [50–53].

#### 4.1.3. Optically-induced fluid flows

So far, we have introduced the thermally-induced flows due to laser irradiation. Here, we introduce fluid flows induced by non-thermal optical effects.

Convection flows can be induced by drag forces exerted on a fluid by particles. A focused beam not only traps the particles but also pushes the particles toward the beam propagation direction. These pushed particles can drag the fluid, resulting in the long-ranged fluid motion that transports the particles toward the focal spot [54]. This type of convection has similar flow patterns with thermal convection, as shown in Fig. 7, but its origin and parameter dependence are completely different.

In [55], the momentum transfer from an optical-vortex laser to a liquid film is demonstrated. Upon the irradiation of the pulse of the optical vortex, the liquid film breaks up and a droplet is ejected. In contrast to other fluid actuation methods as explained above, this method, which we call optical vortex laser induced forward mass

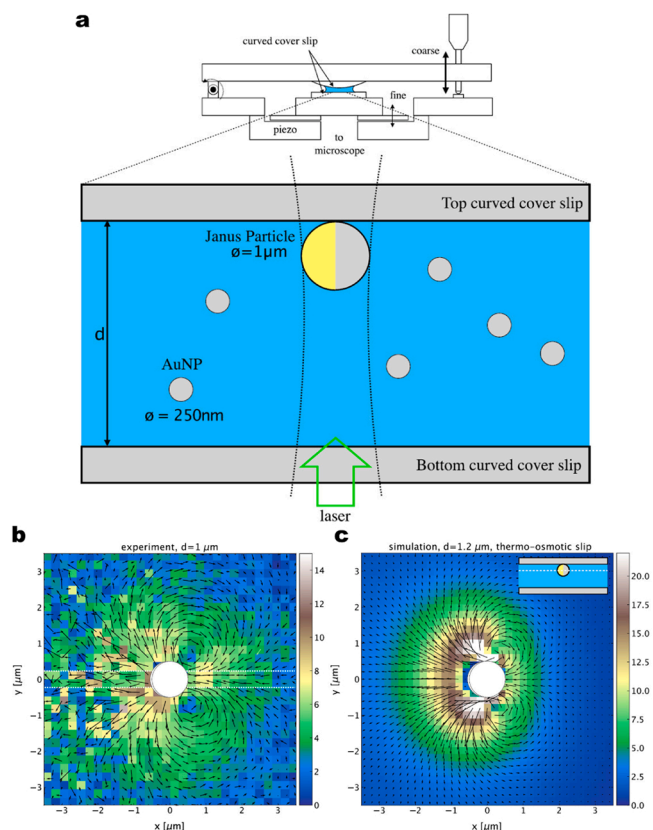


**Fig. 6.** (a) Flow induced around a laser-heated Janus particle. (b) Experimentally-measured velocity from particle tracking of tracers. (c) Velocity obtained by a numerical simulation. Copyright 2019, AIP Publishing. Reprinted with permission from [46].

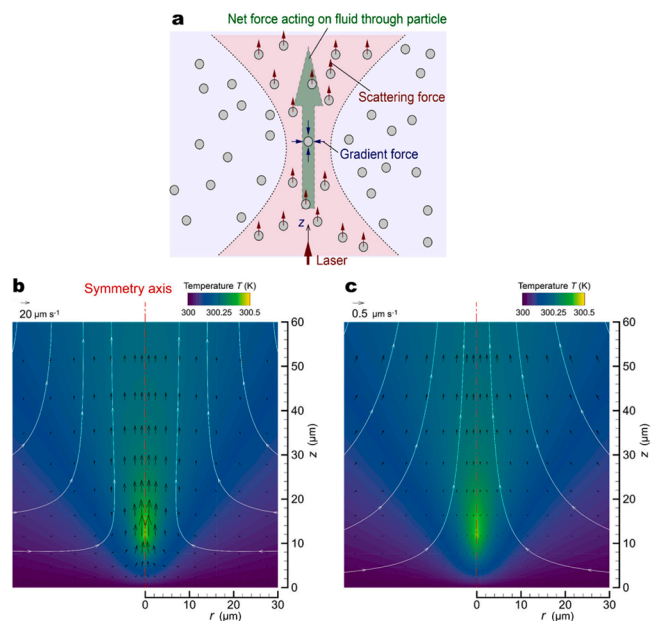


**Fig. 7.** (a) Convection induced by optically-pushed particles [54]. (b) A simulated flow velocity induced by optically-pushed particles. (c) A simulated thermal convection. Note the difference of the flow magnitude and the structure of the streamlines: the flow in (b) is faster and much localized near the laser focus around  $r \approx 0 \mu\text{m}$  and  $z \approx 12 \mu\text{m}$ . Chamber height is  $600 \mu\text{m}$ . Copyright 2020, American Chemical Society. Reprinted with permission from [54].

transfer (OV-LIFT), acts directly on the fluid.

#### 4.2. Forces acting on particles

##### 4.2.1. Hydrodynamic forces

A drag force acting on a target object is the most fundamental effect of fluids. For micro- and nanoscale objects, the effect of inertia can be neglected for both target motion and fluid motion. Usually, we consider a Stokes flow [56] for such a situation. The Stokes flow is characterized by an infinitesimal Reynolds number (the ratio between the fluid inertia and the viscosity) and is also called creeping flows. In short, the Stokes flow is formulated by the Navier-Stokes equation without non-linear terms, which appear as  $(\mathbf{u} \cdot \nabla)\mathbf{u}$  in the left hand side of Eq. (7b).

In [57], it is indeed shown experimentally that the inertia of the particle is not significant in optical trapping. By analyzing the dynamical motion of the particle toward the trapping position based on the balance between the optical gradient force and the fluid drag force, the optical force acting on the particle is experimentally evaluated and numerically examined [57]. The drag force can be used to manipulate target particles hydrodynamically, as shown in Fig. 8. In [58], a couple of micro-rotors are forced to rotate by optical forces. The resulting fluid flows due to rotations are arranged so that the drag force traps or transports target materials as one desires. This can be considered as the localized version of hydrodynamic tweezers [59].

When there are more than two particles in the region of interest, a hydrodynamic interaction, which is a force acting on a particle exerted by others, may play an important role in the collective behavior of the particles. It is reported in [60] that the hydrodynamic interaction induced by Janus particles facilitates the cluster formation of micro-particles. Hydrodynamic interaction may be significant even for much smaller particles. In [61], the orbital motion of 200-nm-diameter particles, which is induced by an optical vortex, can be enhanced by the hydrodynamic interaction. Fig. 9 shows the comparison between the optical vortex experiments and the simulation with hydrodynamic interaction for the 1- $\mu\text{m}$ -diameter particles. In Fig. 9(a), the multiple particles are orbiting in a circular path. Only one of the particles is fluorescent and serves as a tracer. Experimental results on the angular frequency  $\omega$  in Fig. 9(b) and the simulation results in Fig. 9(c) with hydrodynamic interaction both show the positive correlation with respect to the number of particle  $N$  included in the orbital path (see Fig. 9(a)). Note that this experiment used the confinement of 3  $\mu\text{m}$  made of microfabrication (see Sec. 3.2). Thanks to this confinement, the particles are successfully trapped in the orbit, without being pushed out in the beam propagation direction by the scattering force, even for 200-nm-diameter particles. In [62], it is shown numerically that the hydrodynamic interaction between gold nanoparticles generates a uni-directional current even in a periodic optical vortex lattice. For more theoretical descriptions of the motion of small objects in fluids under the presence of others, readers are referred to textbooks [56,63,64].

When a particle is self-rotating in a background fluid flow, a Magnus force acts on the particle in the direction of the cross product of the flow

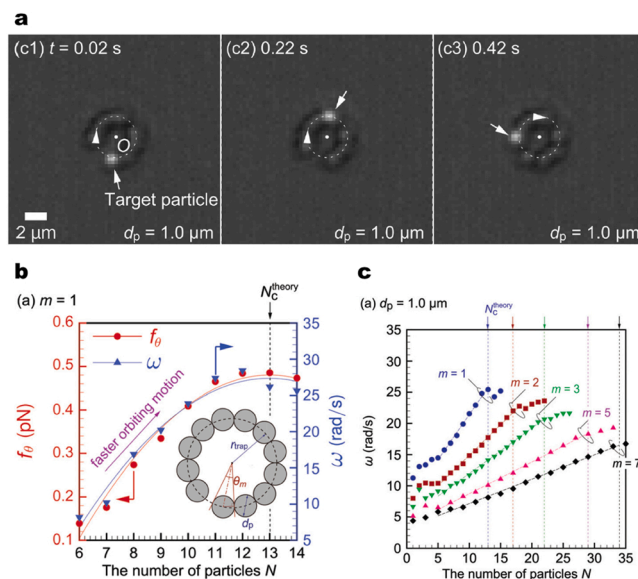


**Fig. 9.** (a) The optical-vortex-induced orbital motion of 1- $\mu\text{m}$ -diameter particles. Many particles are trapped at the same time, one of which is fluorescent as a tagged tracer. (b) The measured optical force (left) and the orbital angular frequency (right) acting on the tagged tracer particle, as a function of the number of particles in the orbit,  $N$ , where the azimuthal mode  $m$  of the optical vortex is set to  $m = 1$ . (c) Corresponding simulation results for various  $m$ . The simulation takes into account hydrodynamic interaction among the particles in the orbit. Chamber height is 3  $\mu\text{m}$ . Reprinted from [61] under the Creative Commons CC BY 3.0 license.

and the rotational axis. This effect is usually negligible for micro flows. However, under the assist of thermophoretic force (see Sec. 4.2.2 below), it is shown in [65] that the optically-trapped, self-rotating, and heated particle is subject to the Magnus force.

##### 4.2.2. Thermal forces

Thermophoretic forces act on dispersed objects in a fluid along a temperature gradient. Phenomenologically, thermophoretic velocity  $V_T$  can be expressed as

$$\mathbf{V}_T = -D_T \nabla T, \quad (8)$$

where  $D_T$  is called thermophoretic mobility and can take both signs. The sign of  $D_T$  is often positive and the magnitude of  $D_T$  is usually reported as  $|D_T| < 10 \mu\text{m}^2 \text{s}^{-1} \text{K}^{-1}$  (see, e.g., [66]). Therefore, when the temperature gradient  $|\nabla T| \approx 1 \text{ K } \mu\text{m}^{-1}$  is created, the thermophoretic speed is estimated as  $10 \mu\text{m s}^{-1}$ . Assuming that the thermophoretic force is counterbalanced by the drag force, we can estimate the magnitude of thermophoretic force as 100 fN, as discussed in Sec. 4.1.1. Therefore, when a strong temperature gradient of the order of  $|\nabla T| \approx 1 \text{ K } \mu\text{m}^{-1}$  is created, thermophoretic forces may become comparable to the optical forces.

This type of thermal force has been applied to various micro- and nanofluidic systems [31,66–72] with a special interest in the thermal manipulation of micro- and nanoscale objects. If a temperature field is created by a photothermal effect, the concentration gradient of the target particles is formed in a steady state as the result of thermophoresis (i.e., a motion induced by thermophoretic forces). To characterize thermophoretic forces in such a situation, a phase and fluorescence microscope can be used for the simultaneous measurement of temperature and concentration of nanoparticles [73]. It should be noted that thermophoretic manipulation can also be exploited using a laser-generated cold region [74]. Thermophoretic forces can be induced effectively when heat sources are localized, that is, a plasmonic heating [38] is promising. In [75], lipid vesicles are manipulated by using such

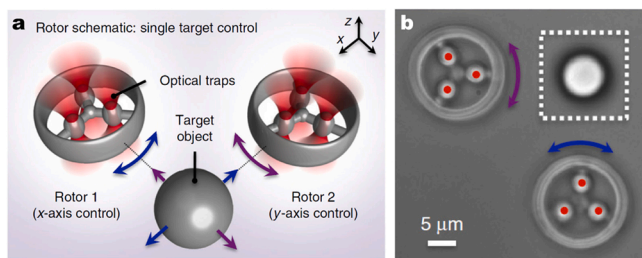


**Fig. 8.** (a) Concept of hydrodynamic manipulation using optically-trapped rotors. (b) Experimental realization of hydrodynamic manipulation. Chamber height is 150  $\mu\text{m}$ . Reprinted from [58] under the Creative Commons CC BY 4.0 license.

thermophoretic forces induced by the heating of a gold thin film. In a similar manner, the heating of a gold thin film is used in [76,77] to induce the thermophoresis of ionic surfactants. These surfactants make concentration gradient fields, which result in a light-induced thermo-electric field that traps a target particle. This type of tweezers is called an optothermoelectric trap and has been applied to various targets, e.g., nanoparticles [78] and Janus particle [79], and also to plasmonic trapping [80]. Fig. 10 shows the optothermoelectric control of micro-swimmers. A Janus particle is heated by the laser irradiation, creating a temperature gradient, as shown in Fig. 10(a). Due to this temperature gradient, charged micelles dispersed in the solution (not shown in the figure) form non-uniform density distribution around the Janus particle. The resulting internal electric field induces self-propelled motion of the Janus particle, as shown in Fig. 10(b).

Thermophoretic force can be used for the crystallization of colloids in a bulk. In [81], a spherical heat source is produced by the laser heating of an optically-trapped titania metal-oxide particle. In a solution, poly(methyl methacrylate) (PMMA) particles are also dispersed. The PMMA particles are refractive-index matched with the solvent and have negative thermophoretic properties. Therefore, without the effect of optical forces, they are attracted thermophoretically to the heat source upon laser irradiation and thus can form a cluster in the bulk. In [82], such a thermophoretic accumulation of organic material to a gold nanoparticle is used to form an organic shell that surrounds the nanoparticle.

As listed above, thermophoresis can elaborate various combinations with optical effects. However, the full understanding of the mechanism is not yet achieved due to physical complexities, although molecular dynamics simulation can give some insights in particular cases [83–85]. If a surrounding fluid is a gas, thermophoretic forces are better understood by using the framework of molecular gas dynamics (see, e.g., [86] and references therein). When a target particle in the air is light-absorbing, the thermal force acting on the particle is especially called a photophoretic force. The photophoretic force can be computed by considering molecular gas flows around a non-uniformly heated particle [87]. Photophoretic forces can be used for the transportation of particles [88] and for the measurement of the mass of the target trapped in air [89]. Recently, a micromachined macroscopic object of centimeter-scale can be levitated by photophoretic force [90], enlarging the range of applications of thermal forces. In [90], the slit-array is fabricated in the centimeter-scale plate-like object, as shown in Fig. 11. Upon light irradiation, one of the faces of the object is heated photo-thermally. The resulting temperature gradient in the slit-array induces the gas flow that levitates the object, as shown in Fig. 11(c).

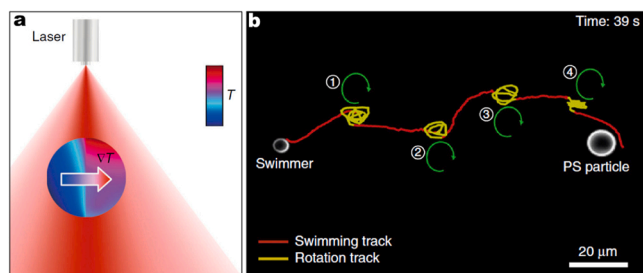


**Fig. 10.** (a) A Janus particle with a diameter of 5  $\mu\text{m}$  attains the temperature gradient upon laser irradiation [79]. Optothermoelectric manipulation enables the Janus particle, a micro-swimmer, to self-propel. Chamber height is 120  $\mu\text{m}$ . Reprinted from [79] under the Creative Commons CC BY 4.0 license.

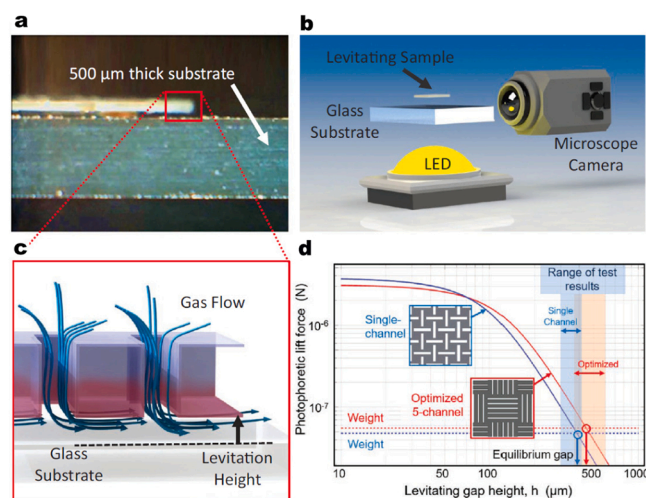


**Fig. 11.** (a) Photophoretic levitation of a macroscopic micromachined object [90]. (b) Schematic of the experiment. (c) Levitation using thermal transpiration, which is the gas flow induced along solid surfaces with temperature gradient. The thermal transpiration is directed from a cold part to a hot part. The object is heated from the bottom by a light illumination, as shown in panel (b). (d) Magnitude of photophoretic lift force predicted by lubrication theory. Copyright 2020, John Wiley and Sons. Reprinted with permission from [90].

## 5. Applications

### 5.1. Separation, trapping, and crystallization enhanced by thermo-fluid dynamics

The combination of the plasmon-enhanced optical force and the thermophoretic force due to the photothermal effect of the plasmon can separate the mixture of DNA with different sizes [91], because these forces have different size-dependencies. It should be remarked that thermophoretic forces acting on target materials are significantly affected by other smaller dispersed materials, e.g., surfactants [69,71, 92]. In particular, it was investigated in [92] that the effects of different surfactants, sodium dodecyl sulfate (SDS) and Triton X-100, on the plasmon-enhanced optical trapping. They found that the trapping efficiency is significantly affected by the thermophoretic characteristics and the molar concentration of the surfactants.

In [93], both optical and thermophoretic forces are used to separate the mixture of core-shell particles with different sizes and thermal conductivity. The smaller core-shell particle has a thick Au shell and thus has large thermal conductivity. On the other hand, the larger core-shell particle has a thin Au shell and low thermal conductivity. Therefore, thermophoretic force is weaker for the smaller particle, because the high-thermal-conductivity particles tend to homogenize the surrounding temperature inhomogeneity, leading to the insufficient temperature gradient. In this case, thermophoretic forces chase the particles away from the laser focus, that is, the larger particles with low thermal conductivity tend to be repelled thermophoretically from the heat. As a result, only a smaller particle can be optically trapped at the laser focus, achieving selective optical trapping.

Thermophoretic force may be accompanied by thermal convection, especially when a channel height is more than tens of micrometers for a water solution (see, e.g., [35]). It was shown in [94] that the photothermal effect of an amorphous silicon layer creates local heating, which induces both thermophoretic force and thermal convection as well as the optical force, reducing the optical power required to trap a microparticle with a diameter of 1.5  $\mu\text{m}$ .

In [95], target particles are tethered at an oil-water interface, as shown in Fig. 12(a). When the optical force traps the first particle on the interface (Fig. 12(b)), a thermo-fluid flow is induced around the particle

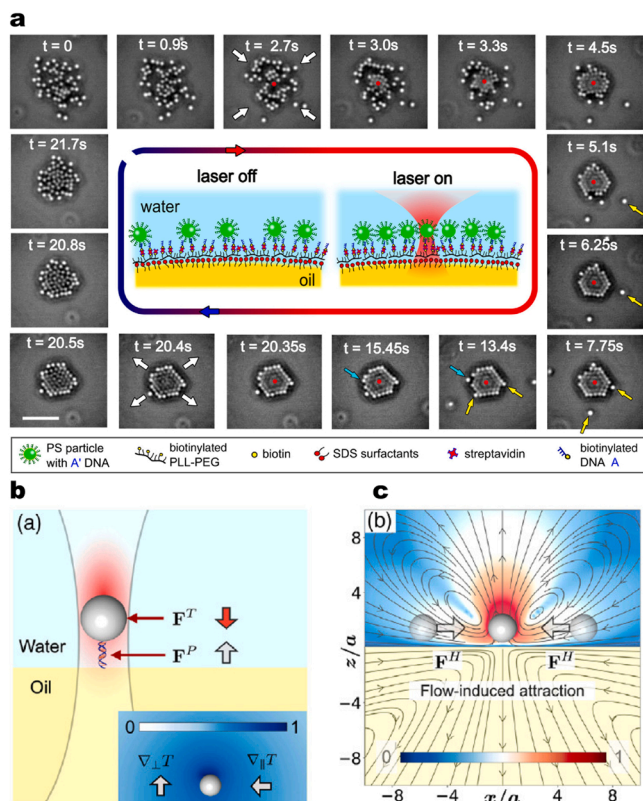


**Fig. 12.** (a) The light-induced crystallization of tethered colloids at an oil-water interface. (b) Optically trapped colloid at the interface and (c) long-ranged optofluidic forces to enhance crystallization. Chamber height is 200  $\mu\text{m}$ . Copyright 2020, American Physical Society. Reprinted with permission from [95].

(Fig. 12(c)). This flow exerts long-range hydrodynamic forces to collect other particles to form the crystal of colloid at the oil-water interface (Fig. 12(a)). Then, short-range optical binding forces [96] crystallize a cluster. Such optical trapping at liquid-liquid interfaces has a new application in photocatalysis. In [97], inorganic nanocrystals, octahedral titania ( $\text{TiO}_2$ ) nanoparticles, are optically trapped at the interface of water and ionic liquid, the latter of which contains  $\text{AuCl}_4^-$ . This anion is reduced by the trapped  $\text{TiO}_2$  particles to generate Au, resulting in the continuous creation of Au particles at the interface.

### 5.2. Sorting of different materials in microfluidic devices

In [98], the competition between a fluid drag force near a micro-channel contraction and a laser-induced thermophoretic force is used to sort the mixture of polystyrene and silica particles with the same diameters. The sorting is possible because the drag forces acting on these two kinds of particles are the same because of the equal diameter, while the thermophoretic forces are not due to different thermophoretic properties. Fig. 13 shows such a situation. The mixture of particles flows from left to right using a pressure difference. However, fluorescent polystyrene particles are repelled from the laser because of thermophoretic force and cannot enter a narrow part (Fig. 13(a)). On the other hand, non-fluorescent silica particles, which are less affected by thermophoresis, can enter into the narrow part (Fig. 13(b)). To achieve this separation, the effect of thermal convection must be avoided, since thermal convection has no function of particle separation. In Fig. 13, the use of microfluidic device with channel height of 7  $\mu\text{m}$  suppressed thermal convection sufficiently.

A microfluidic system is also useful for more engineering applications. For instance, microfluidic sheath flows can be used to prepare

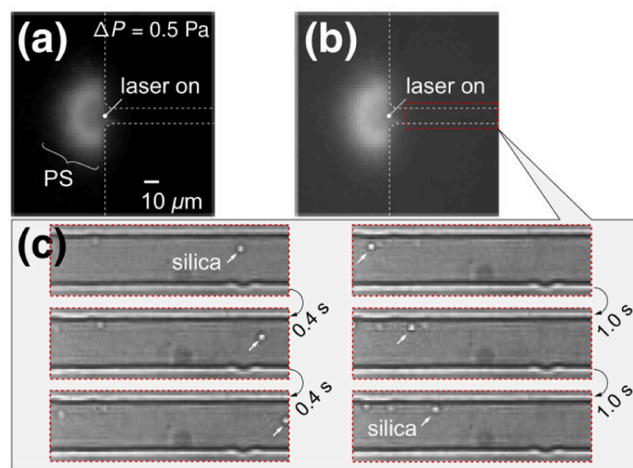


**Fig. 13.** Sorting of the mixture of fluorescent polystyrene (PS) and non-fluorescent silica particles by the laser-induced thermophoresis in microfluidic channel [98]. (a) Dark-field image; only the PS particles are visible. Fluorescent PS particles cannot enter a contraction channel (a narrow part) because the laser at the entrance creates thermophoretic forces that repel the PS particles away. (b,c) Bright-field image; both particles are visible. Only non-fluorescent silica particles can enter the contraction. Reprinted from [98] under the Creative Commons Attribution 4.0 International license.

mono-disperse droplets of right-handed and left-handed chiral microparticles made of liquid crystal [99]. The mixture of these chiral particles can be sorted by using circularly polarized lasers in different directions.

Systematic protocols in microfluidic systems can integrate various functions such as mixers, sorters, sensors, etc., other than optical effects, in a single device and the combination of optical trapping and microfluidics has great advantages in developing novel technologies.

### 5.3. Novel measurement techniques in microfluidic systems using optical tweezers

Optical trapping can develop a new type of flow measurement technique in micro- and nanoscale. In [100], an unsteady flow is induced by the forced oscillation of an optically-trapped microsphere with a diameter of  $\approx 3 \mu\text{m}$ . The flow structure is measured by analyzing the motion of other 30 tracer particles with diameters of 0.5  $\mu\text{m}$ . These tracer particles are arranged in a desired manner by multiple optical potentials.

Optical trapping can also be used to measure the viscosity of a fluid. In [101], a fast viscosity measurement within 20  $\mu\text{s}$  is achieved by the instantaneous velocity measurement of an optically-trapped particle. As demonstrated by these studies [100,101], the optically-trapped particles can be used as a local "probe" that quantifies physical properties or dynamics of fluids.

### 5.4. Measurement of optical trapping force

To evaluate optical forces, several techniques are suggested [14]. Using a liquid flow channel in which a steady flow of low Reynolds number is maintained, the flow velocity to escape an optically trapped microparticle is measured. Here, the viscous drag force and the optical gradient force is equilibrated each other because of the negligibly weak inertial force of the small particle [102].

The liquid motion relative to an optically trapped particle can also be generated using a motorized stage on which a flow chamber is fixed [57, 103,104]. A beam-steering technique using galvanometer scan mirrors is also effective to manipulate the focal point precisely [105].

Measuring optical forces exerted on a small object, an optical force

field and its trapping stiffness are also elucidated. A particle motion in liquids is expressed by the Langevin equation in which thermal fluctuations are represented by Gaussian white noise. Based on the equipartition theorem, the mean square displacement of single particles is  $\langle x^2 \rangle = k_B T / \kappa$ , where  $x$  is the displacement,  $\kappa$  is the trapping stiffness,  $k_B$  is the Boltzmann constant, and  $T$  is the temperature [14]. The displacement of an optically trapped particle was recorded and the stiffness  $\kappa$  was well evaluated [104,106]. The quadratic form of the optical potential was clarified. Wang et al. [103] experimentally evaluated the elasticity of a DNA molecule whose one end is stuck to the coverslip and the other end is fixed to a microparticle optically tweezed.

The differentiation of optical forces and photothermal effects is an important issue in optical trapping. Thermal convection can be eliminated by using a micro and nanoscale confinement, as discussed in Sec. 4. Recently, a nanofluidic device of 300 nm height is used to evaluate optical forces acting on Au nanoparticles [107]. The effect of thermophoresis is more difficult to eliminate. For instance, thermophoresis is observed in a device with a height of  $\approx 7 \mu\text{m}$  although thermal convection is absent in the same device [98]. However, it may be possible to suppress thermophoresis further by using the micro and nanoscale confinement with high-thermal-conductivity material, such as sapphire, to dissipate heat. As for a measurement technique, a novel method to reduce photothermal effect is developed in [108,109]. Here, an optical force between a probing tip and a sample is measured using a heterodyne frequency modulation technique. This enabled successfully the inhibition of the effect of the photothermal expansion of the tip on the force measurement.

### 5.5. Detection and characterization in micro- and nanofluidic devices

Optical fields have been effectively applied to electrical sensing of single nanoparticles and single biomolecules [110,111]. Target objects that are much smaller than the diffraction limit of light can be electrically sensed using nanofluidic channels or nanopores. This method is known as the Coulter counter. When a target particle passes through a comparable-size sensing section, a resistive pulse is usually obtained under an ionic current condition because the electrical conductance drastically decreases due to the volume exclusion effect.

Optical tweezers are applied to the electrical sensing of biomolecules in [112]. The authors precisely measure the electrical force exerted on a DNA molecule that balances with the optical force in a nanopore. A DNA-coated bead, which is optically trapped, approaches a nanopore and the one end of the DNA molecule can be electrically pulled in the nanopore, as shown in Fig. 14(a). As a result, the effective charge of a single base pair is quantitatively evaluated to be  $0.50 \pm 0.05$  elementary charge that corresponded to Manning's charge reduction [113] of 75%, as shown in Fig. 14(b) [112].

Recently, an optical vortex is applied for the electrical measurement of single particles [25,114]. By iteratively passing through a double nanoslit structure, as shown in Fig. 3, the electrical signals of an Au particle are iteratively sensed and the signal-to-noise ratio is drastically improved [25]. The dependence of the particle transport direction and ionic current on the electrical signals are investigated and clarified that resistive or conductive pulses are determined by the relativity of liquid flows, particle transport directions, and electrolyte concentrations.

In [115], a relationship between temperature and optical fields generated by a bowtie-shape Au nanostructure is investigated by measuring the electrical conductance of a nanopore. The authors of [115] find that the temperature linearly increases as the ionic current increases using a 10 mW and 785 nm wavelength laser. Using such a bowtie-shape nanoantenna, a solid-state plasmonic nanopore sensor for the detection of biomolecules is developed in [116]. It is demonstrated that the local heating of Au bowtie nanostructures due to the surface plasmon effectively works to increase the electrical signals of DNA transport, by decreasing the viscosity in the nanopore. Furthermore, it is

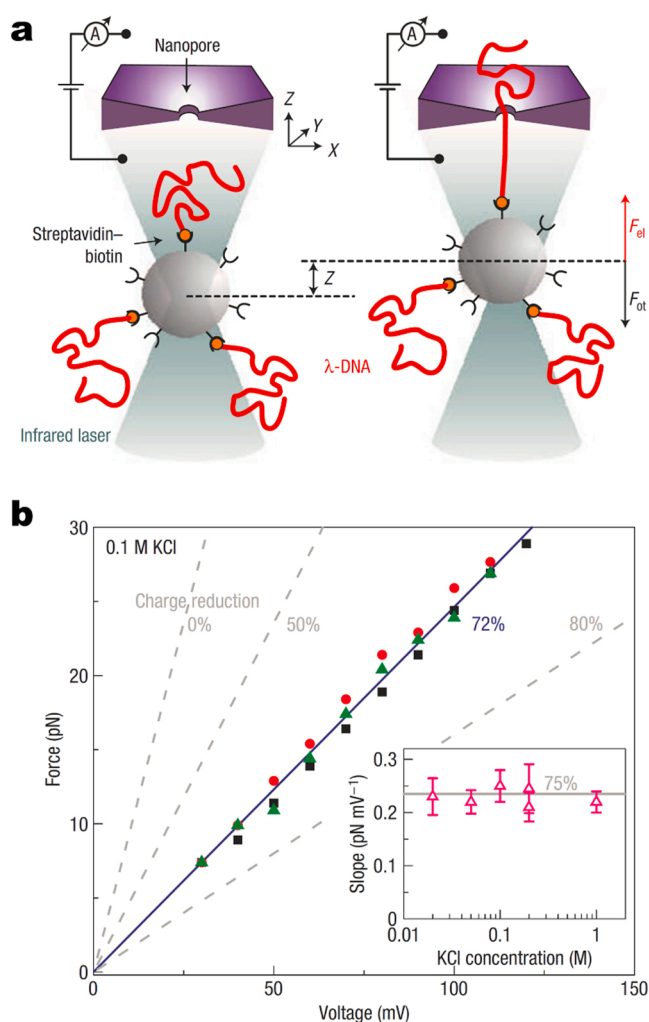


**Fig. 14.** (a) Schematic illustration of a DNA-coated bead near a solid-state nanopore immersed in a saline solution (left image) and a DNA pulled between an electrical force in the nanopore and an optical force, exerted in the opposite directions (right image). (b) The optical force is balanced with the electrical force as a function of applied electric voltage. Copyright 2006, Nature Publishing Group. Reprinted with permission from [112].

suggested that a negative thermophoretic effect induced by the local temperature distribution near the plasmonic nanoantenna in a LiCl solution is effective to attract DNA molecules to a nanopore. It is reported in [117] that a laser irradiation on a nanopore is effective to increase ionic current and also to reduce the translocation speed of target molecules, such as DNA and protein molecules. This is because the laser light induces the surface charges of a nanopore and enhances electroosmotic flows against the target molecules. As mentioned above, the applications of optical fields will also shed light on the frontier of optoelectronic phenomena [118].

## 6. Perspectives

In this mini-review, we introduced recent studies on optical manipulation that utilized thermo-fluid dynamics in micro- and nanosystems. The laser irradiation affected not only target materials but also surrounding fluids and structures, generating heat and triggering flows and forces. The understandings of these side effects were important in the evaluation of optical forces and/or in developing novel functional devices using optical forces.

The flows induced by the laser-irradiation, such as thermal

convection, thermoosmotic flows, Marangoni flows, convection induced by the drag forces of optically-pushed particles, were reviewed along with their applications. These flows could be enhanced by using plasmonic heating techniques, which were well compatible with microfluidic and nanofluidic devices.

The forces acting on target materials, other than optical forces, were described as hydrodynamic or thermal forces. Target particles were interacting with each other through the surrounding fluids, exerting hydrodynamic forces, especially when they were optically accumulated. Hydrodynamic inter-particle effects could affect the collective motion of many particles. On the other hand, thermal forces were less understood theoretically at the moment, but they were actively applied to optothermal manipulations.

Although there have been proposed a variety of applications based on thermo-fluid dynamics in micro- and nanosystems, the fundamental understandings of them are, partially, still far beyond. In particular, the phenomena near interfaces, such as solid-liquid boundaries with temperature variation, liquid-liquid interfaces, and non-uniform electric double layers, need molecular scale description and cannot be understood within macroscopic frameworks. Theoretical and numerical investigations on near-interface phenomena, together with the development of the measurement techniques of flow and thermal fields, should be explored along with their applications.

### Declaration of Competing Interest

The authors declare that they have no known competing financial interests or personal relationships that could have appeared to influence the work reported in this paper.

### Acknowledgements

Researches of our group introduced in this review were supported by Japan Society for the Promotion of Science, Grant-in-Aid for Scientific Research (JSPS KAKENHI) Grant No. 16H06504 in Scientific Research on Innovative Areas 'Nano-Material Optical-Manipulation', No. 18H05242 for Scientific Research (S), No. 18H01372 for Scientific Research (B), No. 20H02067 for Scientific Research (B), No. 15K17973 for Young Scientists (B), No. 18K13687 for Young Scientists, and Japan Science and Technology Agency (JST) CREST Grant No. JPMJCR1903.

### References

- [1] M. Di Ventra, M. Taniguchi, Decoding DNA, RNA and peptides with quantum tunnelling, *Nat. Nanotechnol.* 11 (2) (2016) 117.
- [2] A. Ashkin, Acceleration and trapping of particles by radiation pressure, *Phys. Rev. Lett.* 24 (4) (1970) 156–159.
- [3] A. Ashkin, Applications of laser radiation pressure, *Science* 210 (1980) 1081–1088.
- [4] A. Ashkin, J.M. Dziedzic, J.E. Bjorkholm, S. Chu, Observation of a single-beam gradient force optical trap for dielectric particles, *Opt. Lett.* 11 (5) (1986) 288.
- [5] A. Ashkin, J.M. Dziedzic, T. Yamane, Optical trapping and manipulation of single cells using infrared laser beams, *Nature* 330 (1987) 769–771.
- [6] A. Ashkin, J.M. Dziedzic, Internal cell manipulation using infrared laser traps, *Proc. Natl. Acad. Sci. USA* 86 (20) (1989) 7914–7918.
- [7] A. Ashkin, History of optical trapping and manipulation of small-neutral particle, atoms, and molecules, *IEEE J. Sel. Top. Quantum Electron.* 6 (6) (2000) 841–856.
- [8] P. Jones, O. Marago, G. Volpe, *Optical Tweezers*, Cambridge University Press, 2015.
- [9] K.C. Neuman, S.M. Block, Optical trapping, *Rev. Sci. Instrum.* 75 (9) (2004) 2787–2809.
- [10] A. Ashkin, Forces of a single-beam gradient laser trap on a dielectric sphere in the ray optics regime, *Biophys. J.* 61 (1992) 569–582.
- [11] G.J. Sonek, W. Wang, Theory of optical trapping forces: a review, *Rev. Laser Eng.* 24 (11) (1996) 1139–1147.
- [12] K. Svoboda, S.M. Block, Optical trapping of metallic rayleigh particles, *Opt. Lett.* 19 (13) (1994) 930–932.
- [13] L. Jauffred, S.M.-R. Taheri, R. Schmitt, H. Linke, L.B. Oddershede, Optical trapping of gold nanoparticles in air, *Nano Lett.* 15 (7) (2015) 4713–4719.
- [14] K. Svoboda, S. Block, Biological applications of optical forces, *Annu. Rev. Biophys. Biomol. Struct.* 23 (1994) 247–285.
- [15] Y. Harada, T. Asakura, Radiation forces on a dielectric sphere in the Rayleigh scattering regime, *Opt. Commun.* 124 (1996) 529–541.
- [16] A. Ramos, H. Morgan, N.G. Green, A. Castellanos, Ac electrokinetics: a review of forces in microelectrode structures, *J. Phys. D: Appl. Phys.* 31 (18) (1998) 2338–2353.
- [17] K.-N. Liou, J.E. Hansen, Intensity and polarization for single scattering by polydisperse sphere: a comparison of ray optics and Mie theory, *J. Atmos. Sci.* 28 (1971) 995–1004.
- [18] D.J. Gordon, Mie scattering by optically active particles, *Biochemistry* 11 (3) (1972) 413–420.
- [19] K. Ren, G. Gréhan, G. Gouesbet, Prediction of reverse radiation pressure by generalized Lorenz-Mie theory, *Appl. Opt.* 35 (1996) 2702–2710.
- [20] Y. Xu, Nanofluidics: a new arena for materials science, *Adv. Mater.* 30 (3) (2017), 1702419.
- [21] N.-T. Nguyen, S.T. Wereley, S.A.M. Shaegh, *Fundamentals and applications of microfluidics*, Artech House, 2019.
- [22] G.A. Cooksey, P.N. Patrone, J.R. Hands, S.E. Meek, A.J. Kearsley, Dynamic measurement of nanoflows: realization of an optofluidic flow meter to the nanoliter-per-minute scale, *Anal. Chem.* 91 (16) (2019) 10713–10722.
- [23] P.N. Patrone, G. Cooksey, A. Kearsley, Dynamic measurement of nanoflows: analysis and theory of an optofluidic flowmeter, *Phys. Rev. Appl.* 11 (3) (2019), 034025.
- [24] T. Tsuji, Y. Matsumoto, S. Kawano, Flow with nanoparticle clustering controlled by optical forces in quartz glass nanoslits, *Microfluid. Nanofluid.* 23 (11) (2019) 126.
- [25] R. Nakatsuka, S. Yanai, K. Nakajima, K. Doi, S. Kawano, Electrical sensing of Au nanoparticles manipulated by an optical vortex, *J. Phys. Chem. C* 125 (17) (2021) 9507–9515.
- [26] S. Ghosh, A. Ghosh, All optical dynamic nanomanipulation with active colloidal tweezers, *Nat. Commun.* 10 (2019) 4191.
- [27] B. Ciraulo, J. Garcia-Guirado, I. de Miguel, J.O. Arroyo, R. Quidant, Long-range optofluidic control with plasmon heating, *Nat. Commun.* 12 (2021) 2001.
- [28] H. Bruus, *Theoretical microfluidics*, Oxford University Press, Oxford, 2008.
- [29] L.D. Landau, E.M. Lifshitz, *Fluid Mechanics*, Butterworth-Heinemann, 1987.
- [30] M. Lappa, *Thermal convection: patterns, evolution and stability*, John Wiley & Sons, 2009.
- [31] T. Tsuji, S. Saita, S. Kawano, Dynamic pattern formation of microparticles in a uniform flow by an on-chip thermophoretic separation device, *Phys. Rev. Appl.* 9 (2) (2018), 024035.
- [32] G.M. Hale, M.R. Querry, Optical constants of water in the 200-nm to 200- $\mu$ m wavelength region, *Appl. Opt.* 12 (3) (1973) 555.
- [33] S. Ito, T. Sugiyama, N. Toitani, G. Katayama, H. Miyasaka, Application of fluorescence correlation spectroscopy to the measurement of local temperature in solutions under optical trapping condition, *J. Phys. Chem. B* 111 (9) (2007) 2365–2371.
- [34] D. Rivière, B. Selva, H. Chraïbi, U. Delabre, J.-P. Delville, Convection flows driven by laser heating of a liquid layer, *Phys. Rev. E* 93 (2) (2016), 023112.
- [35] T. Tsuji, S. Taguchi, H. Takamatsu, Switching between laser-induced thermophoresis and thermal convection of liquid suspension in a microgap with variable dimension, *Electrophoresis* 42 (21–22) (2021) 2401–2409.
- [36] Y. Qian, S.L. Neale, J.H. Marsh, Microparticle manipulation using laser-induced thermophoresis and thermal convection flow, *Sci. Rep.* 10 (2020) 19169.
- [37] D. Zablotsky, M.M. Maiorov, Optofluidic microconvection with magnetic nanoparticles: novel interaction of thermal diffusion and magnetic field, *Int. J. Heat. Mass Transf.* 164 (2021), 120552.
- [38] G. Baffou, *Thermoplasmonics*, Cambridge University Press, 2017.
- [39] K. Hayashi, Y. Yamamoto, M. Tamura, S. Tokonami, T. Iida, Damage-free light-induced assembly of intestinal bacteria with a bubble-mimetic substrate, *Commun. Biol.* 4 (2021) 385.
- [40] J.C. Ndukaife, A.V. Kildishev, A.G.A. Nnanna, V.M. Shalaev, S.T. Wereley, A. Boltasseva, Long-range and rapid transport of individual nano-objects by a hybrid electrothermoplasmonic nanotweezer, *Nat. Nanotechnol.* 11 (1) (2016) 53.
- [41] C. Hong, S. Yang, J.C. Ndukaife, Stand-off trapping and manipulation of sub-10 nm objects and biomolecules using opto-thermo-electrohydrodynamic tweezers, *Nat. Nanotechnol.* 15 (11) (2020) 908–913.
- [42] B. Derjaguin, N. Churaev, M. Muller, *Surface Forces*, Springer, 1987.
- [43] S.R. De Groot, P. Mazur, *Non-equilibrium thermodynamics*, Dover, 1984.
- [44] A.P. Bregulla, A. Würger, K. Günther, M. Mertig, F. Cichos, Thermo-osmotic flow in thin films, *Phys. Rev. Lett.* 116 (18) (2016), 188303.
- [45] X. Lou, N. Yu, R. Liu, K. Chen, M. Yang, Dynamics of a colloidal particle near a thermoosmotic wall under illumination, *Soft Matter* 14 (2018) 1319–1326.
- [46] A.P. Bregulla, F. Cichos, Flow fields around pinned self-thermophoretic microswimmers under confinement, *J. Chem. Phys.* 151 (4) (2019), 044706.
- [47] S. Auschra, A. Bregulla, K. Kroy, F. Cichos, Thermotaxis of Janus particles, *Eur. Phys. J. E* 44 (7) (2021) 90.
- [48] E. Avital, T. Miloh, Self-thermophoresis of laser-heated spherical Janus particles, *Eur. Phys. J. E* 44 (11) (2021) 139.
- [49] T. Miloh, Light-induced thermoosmosis about conducting ellipsoidal nanoparticles, *Proc. R. Soc. A* 475 (2223) (2019), 20180040.
- [50] K. Namura, K. Nakajima, K. Kimura, M. Suzuki, Photothermally controlled Marangoni flow around a micro bubble, *Appl. Phys. Lett.* 106 (4) (2015), 043101.
- [51] K. Setoura, S. Ito, H. Miyasaka, Stationary bubble formation and Marangoni convection induced by cw laser heating of a single gold nanoparticle, *Nanoscale* 9 (2016) 719–730.
- [52] A. Miniewicz, S. Bartkiewicz, H. Orlikowska, K. Dradrach, Marangoni effect visualized in two-dimensions optical tweezers for gas bubbles, *Sci. Rep.* 6 (2016) 34787.

- [53] J. Chikazawa, T. Uwada, A. Furube, S. Hashimoto, Flow-induced transport via optical heating of a single gold nanoparticle, *J. Phys. Chem. C* 123 (7) (2019) 4512–4522.
- [54] C. Hosokawa, T. Tsuji, T. Kishimoto, T. Okubo, S.N. Kudoh, S. Kawano, Convection dynamics forced by optical trapping with a focused laser beam, *J. Phys. Chem. C* 124 (15) (2020) 8323–8333.
- [55] R. Nakamura, H. Kawaguchi, M. Iwata, A. Kaneko, R. Nagura, S. Kawano, K. Toyoda, K. Miyamoto, T. Omatsu, Optical vortex-induced forward mass transfer: manifestation of helical trajectory of optical vortex, *Opt. Express* 27 (26) (2019) 38019.
- [56] J. Happel, H. Brenner, *Low Reynolds number hydrodynamics: with special applications to particulate media*, Martinus Nijhoff Publishers, 1983.
- [57] F. Nito, T. Shiozaki, R. Nagura, T. Tsuji, K. Doi, C. Hosokawa, S. Kawano, Quantitative evaluation of optical forces by single particle tracking in slit-like microfluidic channels, *J. Phys. Chem. C* 122 (31) (2018) 17963–17975.
- [58] U.G. Büttai, G.M. Gibson, Y.-L.D. Ho, M. Taverne, J.M. Taylor, D.B. Phillips, Indirect optical trapping using light driven micro-rotors for reconfigurable hydrodynamic manipulation, *Nat. Commun.* 10 (2019) 1215.
- [59] A. Shenoy, C.V. Rao, C.M. Schroeder, Stokes trap for multiplexed particle manipulation and assembly using fluidics, *Proc. Natl. Acad. Sci. USA* 113 (15) (2016) 3976–3981.
- [60] S.M. Mousavi, I. Kasianiuk, D. Kasyanyuk, S.K. Velu, A. Callegari, L. Biancofiore, G. Volpe, Clustering of Janus particles in optical potential driven by hydrodynamic fluxes, *Soft Matter* 15 (28) (2019) 5748–5759.
- [61] T. Tsuji, R. Nakatsuka, K. Nakajima, K. Doi, S. Kawano, Effect of hydrodynamic inter-particle interaction on the orbital motion of dielectric nanoparticles driven by an optical vortex, *Nanoscale* 12 (12) (2020) 6673–6690.
- [62] R. Delgado-Buscailioni, M. Meléndez, J. Luis-Hita, M.I. Marqués, J.J. Sáenz, Emergence of collective dynamics of gold nanoparticles in an optical vortex lattice, *Phys. Rev. E* 98 (6) (2018), 062614.
- [63] S. Kim, S.J. Karrila, *Microhydrodynamics: principles and selected applications*, Dover, 2005.
- [64] M.D. Graham, *Microhydrodynamics, Brownian Motion, and Complex Fluids*, Cambridge University Press, 2018.
- [65] M. Romodina, N. Shchelkunov, E. Lyubin, A. Fedyanin, Thermophoresis-assisted micro-scale Magnus effect in optical traps, *JETP Lett.* 110 (11) (2019) 750–754.
- [66] R. Piazza, Thermophoresis: moving particles with thermal gradients, *Soft Matter* 4 (9) (2008) 1740–1744.
- [67] S. Dühr, D. Braun, Why molecules move along a temperature gradient, *Proc. Natl. Acad. Sci. USA* 103 (52) (2006) 19678–19682.
- [68] R. Piazza, A. Parola, Thermophoresis in colloidal suspensions, *J. Phys.: Condens. Matter* 20 (15) (2008), 153102.
- [69] H.-R. Jiang, H. Wada, N. Yoshinaga, M. Sano, Manipulation of colloids by a nonequilibrium depletion force in a temperature gradient, *Phys. Rev. Lett.* 102 (20) (2009), 208301.
- [70] D. Vigolo, R. Rusconi, H.A. Stone, R. Piazza, Thermophoresis: microfluidics characterization and separation, *Soft Matter* 6 (15) (2010) 3489–3493.
- [71] Y.T. Maeda, A. Buguin, A. Libchaber, Thermal separation: interplay between the Soret effect and entropic force gradient, *Phys. Rev. Lett.* 107 (3) (2011), 038301.
- [72] T. Tsuji, K. Kozai, H. Ishino, S. Kawano, Direct observations of thermophoresis in microfluidic systems, *Micro Nano Lett.* 12 (8) (2017) 520–525.
- [73] S. Shakib, B. Rogez, S. Khadir, J. Polleux, A. Würger, G. Baffou, Microscale thermophoresis in liquids induced by plasmonic heating and characterized by phase and fluorescence microscopies, *J. Phys. Chem. C* 125 (39) (2021) 21533–21542.
- [74] J. Li, Z. Chen, Y. Liu, P.S. Kollipara, Y. Feng, Z. Zhang, Y. Zheng, Opto-refrigerative tweezers, *Sci. Adv.* 7 (26) (2021), eabh1101.
- [75] E.H. Hill, J. Li, L. Lin, Y. Liu, Y. Zheng, Opto-thermophoretic attraction, trapping, and dynamic manipulation of lipid vesicles, *Langmuir* 34 (44) (2018) 13252–13262.
- [76] L. Lin, J. Zhang, X. Peng, Z. Wu, A.C. Coughlan, Z. Mao, M.A. Bevan, Y. Zheng, Opto-thermophoretic assembly of colloidal matter, *Sci. Adv.* 3 (9) (2017), e1700458.
- [77] L. Lin, E.H. Hill, X. Peng, Y. Zheng, Optothermal manipulations of colloidal particles and living cells, *Acc. Chem. Res.* 51 (6) (2018) 1465–1474.
- [78] L. Lin, M. Wang, X. Peng, E.N. Lissek, Z. Mao, L. Scarabelli, E. Adkins, S. Coskun, H.E. Unalan, B.A. Korgel, L.M. Liz-Marzán, E.-L. Florin, Y. Zheng, Opto-thermoelectric nanotweezers, *Nat. Photonics* 12 (4) (2018) 195–201.
- [79] X. Peng, Z. Chen, P.S. Kollipara, Y. Liu, J. Fang, L. Lin, Y. Zheng, Opto-thermoelectric microswimmers, *Light: Sci. Appl.* 9 (2020) 141.
- [80] Y. Liu, L. Lin, B. Bangalore Rajeeva, J. Jarrett, X. Li, X. Peng, P. Kollipara, K. Yao, D. Akinwande, A.K. Dunn, Y. Zheng, Nanoradiator-mediated deterministic opto-thermoelectric manipulation, *ACS Nano* 12 (10) (2018) 10383–10392.
- [81] N. Bruot, H. Tanaka, Externally driven local colloidal ordering induced by a pointlike heat source, *Phys. Rev. Res.* 1 (3) (2019), 033200.
- [82] M. Enders, S. Mukai, T. Uwada, S. Hashimoto, Plasmonic nanofabrication through optical heating, *J. Phys. Chem. C* 120 (12) (2016) 6723–6732.
- [83] T. Tsuji, H. Iseki, I. Hanasaki, S. Kawano, Negative thermophoresis of nanoparticles interacting with fluids through a purely-repulsive potential, *J. Phys.: Condens. Matter* 29 (47) (2017), 475101.
- [84] X. Peng, L. Lin, E.H. Hill, P. Kunal, S.M. Humphrey, Y. Zheng, Opto-thermophoretic manipulation of colloidal particles in nonionic liquids, *J. Phys. Chem. C* 122 (42) (2018) 24226–24234.
- [85] H. Ding, P.S. Kollipara, L. Lin, Y. Zheng, Atomistic modeling and rational design of optothermal tweezers for targeted applications, *Nano Res.* 14 (1) (2021) 295–303.
- [86] Y. Sone, *Molecular gas dynamics: theory, techniques, and applications*, Birkhäuser Boston, 2007.
- [87] Y. Sone, K. Aoki, Forces on a spherical particle in a slightly rarefied gas, in: J. L. Potter (Ed.), *Rarefied Gas Dynamics*, vol. 51, AIAA, New York, 1977, pp. 417–433.
- [88] V.G. Shvedov, A.V. Rode, Y.V. Izdebskaya, A.S. Desyatnikov, W. Krolikowski, Y. S. Kivshar, Giant optical manipulation, *Phys. Rev. Lett.* 105 (11) (2010), 118103.
- [89] S.K. Bera, A. Kumar, S. Sil, T.K. Saha, T. Saha, A. Banerjee, Simultaneous measurement of mass and rotation of trapped absorbing particles in air, *Opt. Lett.* 41 (18) (2016) 4356–4359.
- [90] J. Cortes, C. Stanczak, M. Azadi, M. Narula, S.M. Nicaise, H. Hu, I. Bargatin, Photophoretic levitation of macroscopic nanocardboard plates, *Adv. Mater.* 32 (16) (2020), 1906878.
- [91] T. Shoji, K. Itoh, J. Saitoh, N. Kitamura, T. Yoshii, K. Murakoshi, Y. Yamada, T. Yokoyama, H. Ishihara, Y. Tsuboi, Plasmonic manipulation of DNA using a combination of optical and thermophoretic forces: Separation of different-sized DNA from mixture solution, *Sci. Rep.* 10 (2020) 3349.
- [92] Q. Jiang, B. Rogez, J.-B. Claude, G. Baffou, J. Wenger, Quantifying the role of the surfactant and the thermophoretic force in plasmonic nano-optical trapping, *Nano Lett.* 20 (12) (2020) 8811–8817.
- [93] K. Setoura, T. Tsuji, S. Ito, S. Kawano, H. Miyasaka, Opto-thermophoretic separation and trapping of plasmonic nanoparticles, *Nanoscale* 11 (44) (2019) 21093–21102.
- [94] J.A. Zenteno-Hernandez, J.V. Lozano, J.A. Sarabia-Alonso, J. Ramírez-Ramírez, R. Ramos-García, Optical trapping in the presence of laser-induced thermal effects, *Opt. Lett.* 45 (14) (2020) 3961–3964.
- [95] A. Caciagli, R. Singh, D. Joshi, R. Adhikari, E. Eiser, Controlled optofluidic crystallization of colloids tethered at interfaces, *Phys. Rev. Lett.* 125 (2020), 068001.
- [96] M.-T. Wei, J. Ng, C.T. Chan, H.D. Ou-Yang, Lateral optical binding between two colloidal particles, *Sci. Rep.* 6 (2016) 38883.
- [97] Y. Tsuboi, S. Naka, D. Yamanishi, T. Nagai, K. Yuyama, T. Shoji, B. Ohtani, M. Tamura, T. Iida, T. Kameyama, T. Torimoto, Optical trapping of nanocrystals at oil/water interfaces: Implications for photocatalysis, *ACS Appl. Nano Mater.* 4 (11) (2021) 11743–11752.
- [98] T. Tsuji, Y. Sasai, S. Kawano, Thermophoretic manipulation of micro- and nanoparticle flow through a sudden contraction in a microchannel with near-infrared laser irradiation, *Phys. Rev. Appl.* 10 (4) (2018), 044005.
- [99] N. Kravets, A. Aleksanyan, H. Chraïbi, J. Leng, E. Brasselet, Optical enantioseparation of racemic emulsions of chiral microparticles, *Phys. Rev. Appl.* 11 (4) (2019), 044025.
- [100] N. Bruot, P. Cicuta, H. Bloomfield-Gadêlha, R.E. Goldstein, J. Kotar, E. Lauga, F. Nadal, Direct measurement of unsteady microscale Stokes flow using optically driven microspheres, *Phys. Rev. Fluids* 6 (2021), 053102.
- [101] L.S. Madsen, M. Waleed, C.A. Casacio, A. Terrasson, A.B. Stilgoe, M.A. Taylor, W. P. Bowen, Ultrafast viscosity measurement with ballistic optical tweezers, *Nat. Photonics* 15 (5) (2021) 386–392.
- [102] H. Liang, W. Wright, C. Rieder, E. Salmon, G. Profeta, J. Andrews, Y. Liu, G. Sonek, M. Berns, Directed movement of chromosome arms and fragments in mitotic newt lung cells using optical scissors and optical tweezers, *Exp. Cell Res.* 213 (1994) 308–312.
- [103] M.D. Wang, H. Yin, R. Landick, J. Gelles, S.M. Block, Stretching DNA with optical tweezers, *Biophys. J.* 72 (1997) 1335–1346.
- [104] N. Malagnino, G. Pesce, A. Sasso, E. Arimondo, Measurements of trapping efficiency and stiffness in optical tweezers, *Opt. Commun.* 214 (2002) 15–24.
- [105] M. Dienerowitz, M. Mazilu, K. Dholakia, Optical manipulation of nanoparticles: a review, *J. Nanophotonics* 2 (2008), 021875.
- [106] K. Doi, F. Nito, R. Koyama, S. Kawano, Repetitive electrical sensing of optically trapped microparticles in motorized liquid flows, *J. Phys. Chem. C* 124 (19) (2020) 10627–10637.
- [107] K. Nakajima, T. Tsujimura, K. Doi, S. Kawano, Visualization of optical vortex forces acting on Au nanoparticles transported in nanofluidic channels, *ACS Omega* 7 (3) (2022) 2638–2648.
- [108] J. Yamanishi, Y. Naitoh, Y. Li, Y. Sugawara, Heterodyne frequency modulation in photoinduced force microscopy, *Phys. Rev. Appl.* 9 (2) (2018), 024031.
- [109] J. Yamanishi, H. Yamane, Y. Naitoh, Y.J. Li, N. Yokoshi, T. Kameyama, S. Koyama, T. Torimoto, H. Ishihara, Y. Sugawara, Optical force mapping at the single-nanometre scale, *Nat. Commun.* 12 (2021) 3865.
- [110] C. Dekker, Solid-state nanopores, *Nat. Nanotechnol.* 2 (4) (2007) 209–215.
- [111] M. Zwolak, M. Di Ventra, Colloquium: physical approaches to DNA sequencing and detection, *Rev. Mod. Phys.* 80 (2008) 141–165.
- [112] U.F. Keyser, B.N. Koeleman, S. van Dorp, D. Krapf, R.M.M. Smeets, S.G. Lemay, N. H. Dekker, C. Dekker, Direct force measurements on DNA in a solid-state nanopore, *Nat. Phys.* 2 (7) (2006) 473–477.
- [113] G. Manning, On the application of polyelectrolyte “limiting law” to the helix-coil transition of DNA. i. excess univalent cations, *Biopolymers* 11 (1972) 937–949.
- [114] K. Nakajima, R. Nakatsuka, T. Tsuji, K. Doi, S. Kawano, Synchronized resistive-pulse analysis with flow visualization for single micro- and nanoscale objects driven by optical vortex in double orifice, *Sci. Rep.* 11 (2021) 9323.
- [115] M.P. Jonsson, C. Dekker, Plasmonic nanopore for electrical profiling of optical intensity landscapes, *Nano Lett.* 13 (2013) 1029–1033.

- [116] F. Nicoli, D. Verschuere, M. Klein, C. Dekker, M.P. Jonsson, DNA translocations through solid-state plasmonic nanopores, *Nano Lett.* 14 (2014) 6917–6925.
- [117] N. Di Fiori, A. Squires, D. Bar, T. Gilboa, T.D. Moustakas, A. Meller, Optoelectronic control of surface charge and translocation dynamics in solid-state nanopores, *Nat. Nanotechnol.* 8 (12) (2013) 946–951.
- [118] T. Gilboa, A. Meller, Optical sensing and analyte manipulation in solid-state nanopores, *Analyst* 140 (2015) 4733–4747.



**Tetsuro Tsuji** received B.S., M.S., and Ph.D. degrees from the Department of Mechanical Engineering and Science, Kyoto University, Japan, in 2008, 2010, and 2013, respectively. Following graduation, he was an Assistant Professor at Osaka University. In the year 2019, he was appointed as an Assistant Professor in the Department of Advanced Mathematical Sciences, Graduate School of Informatics, Kyoto University. He has been an Associate Professor since 2021 in the same department. His current research area is fluid dynamics in the micro and nanoscales and molecular fluid dynamics.



**Kentaro Doi** received B.S., M.S., and Ph.D. degrees from the Department of Engineering, Kyoto University, Japan, in 2001, 2003, and 2007, respectively. His career started as an Assistant Professor of Kyoto University from 2004 to 2007; he was promoted as an Associate Professor from 2007 to 2019 in the Department of Mechanical Science and Bioengineering, Osaka University. Since 2020, he has been a Professor in the Department of Mechanical Engineering, Toyohashi University of Technology. His current research interest is micro- and nanoscale thermo-fluid engineering and ion transport phenomena coupling with quantum molecular dynamics.



**Satoyuki Kawano** received B.S., M.S., and Ph.D. degrees in Mechanical Engineering from Tohoku University, Japan, in 1987, 1989, and 1992, respectively. Following graduation, he was a Postdoctoral Fellow of the Japan Society for the Promotion of Science in 1992. He was appointed as a Research Associate in 1993 and as an Associate Professor in 1996 at Tohoku University. In the year 2005, he was appointed as a Professor at Osaka University. His current research interest is micro and nanoscale fluid dynamics about micromachined artificial organs and single-molecule measurements.